SCIENCE CHINA
Physics, Mechanics & Astronomy

• Article •

May 2012 Vol.55 No.5: 844–853
doi: 10.1007/s11433-012-4702-0

Optimization of the MUSCL scheme by dispersion and dissipation

LENG Yan[1], LI XinLiang[1*], FU DeXun[2] & MA YanWen[2]

[1] *The State Key Laboratory of High-temperature Gas Dynamics (LHD), Institute of Mechanics, Chinese Academy of Sciences, Beijing 100190, China;*
[2] *The State Key Laboratory of Nonlinear Mechanics (LNM), Institute of Mechanics, Chinese Academy of Sciences, Beijing 100190, China*

Received May 20, 2011; accepted October 11, 2011; published online March 26, 2012

A second-order optimized monotonicity-preserving MUSCL scheme (OMUSCL2) is developed based on the dispersion and dissipation optimization and monotonicity-preserving technique. The new scheme (OMUSCL2) is simple in expression and is easy for use in CFD codes. Compared with the original second-order or third-order MUSCL scheme, the new scheme shows nearly the same CPU cost and higher resolution to shockwaves and small-scale waves. This new scheme has been tested through a set of one-dimensional and two-dimensional tests, including the Shu-Osher problem, the Sod problem, the Lax problem, the two-dimensional double Mach reflection and the RAE2822 transonic airfoil test. All numerical tests show that, compared with the original MUSCL schemes, the new scheme causes fewer dispersion and dissipation errors and produces higher resolution.

MUSCL scheme, monotonicity-preserving, resolution, dissipation/dispersion error, optimization

PACS number(s): 47.11.DF, 47.27.E-

Citation: Leng Y, Li X L, Fu D X, et al. Optimization of the MUSCL scheme by dispersion and dissipation. Sci China-Phys Mech Astron, 2012, 55: 844–853, doi: 10.1007/s11433-012-4702-0

Computational fluid dynamics (CFD) plays an important role in the aerospace engineering, and one of its main tasks is to develop a high resolution scheme [1]. Generally speaking, the resolution of numerical solution means the ability to describe flow characteristics which attract us. High resolution scheme [1] means that the numerical solution of this scheme can give a sharp and vivid picture to the flow characteristics which are in the range of interesting physical scale. This scale usually contains a small-scale flow structure which is difficult to simulate correctly. For shock waves, the resolution means the numerical shock is sharp and the flow variables (such as density, velocity, and pressure) have no or small oscillation through shock. When the shock wave is generated in the flow field, the characteristic scale of flow structure shows a sharp discrepancy among different regions [2]. The characteristic scale of inviscid shock is zero, while the characteristic scale of flow is finite. Furthermore, flow variables are discontinuous through shock. All of these cause difficulties in numerical calculation. A good scheme should be high in resolution and strong in ability to capture shock for multi-scale complex flow (e.g. turbulence) with shock. In addition, numerical solution should be free from non-physical high frequency oscillation near the shock, and different scale physical parameters can't be polluted through shock wave. Therefore, it's necessary to develop high resolution schemes for engineering application.

Numerical simulation of shock has made significant progress since the 1980s. In 1983, Harten [1] introduced the concept of total variation diminishing (TVD), and came up with a second order TVD scheme. Based on Harten's TVD concept and condition [1], limiters can be defined to restore the TVD property of the scheme and to prevent the non-physical oscillations near the discontinuities. TVD limiters are bounded non-linear functions following Harten's TVD condition. These limiters ensure that any reconstructed values at any time don't lie outside the range of the initial

*Corresponding author (email: lixl@imech.ac.cn)

data [3]. Sweby [4] proposed a series of second order TVD schemes using the flux limiters. In addition, Van Leer [5] developed a high-resolution method called MUSCL (monotonic upstream-centered scheme for conservation law). This method first extrapolated interface values by using the cell averages, and then generated flux through the flux splitting technique. This avoids under and overshoots phenomena and leads to a maximum principle on the discrete solution. MUSCL methods are one of the most popular second-order or third-order finite volume methods. Although TVD schemes show highly efficient and stable shock capturing ability, the order in the local extreme point is only first-order for satisfying the TVD property. To avoid this drawback, Harten [6] introduced the essentially non-oscillatory concept (ENO). Then many researchers have constructed high-order ENO [6,7] and WENO [7,8] schemes. There are also the total variation bounded (TVB) [9] method and monotonicity-preserving (MP) [10] method. However, more stencil points are used in high-order (more than three-order) schemes, and this limits the flexibility in complex geometries.

The finite volume method (FVM) is widely used in engineering applications due to its simplicity for complex geometries and built-in conservative property. To be flexible for complex geometries, the scheme stencil in most FVM codes are four points, i.e. four points are used to compute the face value $U_{I+1/2}$. For engineering CFD codes, the MUSCL scheme is one of the most popular schemes to compute $U_{I+1/2}$. This scheme is modified from the base schemes by using limiter techniques. The base schemes of MUSCL are the second-order central scheme, the second-order upwind scheme, and the third-order upwind scheme or the Fromm scheme. Although the MUSCL scheme contains many good properties, it still has room for optimization. For example, four points are used to compute $U_{I+1/2}$, and only three points are used to compute the Left and the Right face values $U^L_{I+1/2}$, $U^R_{I+1/2}$. The message of one point is not used in the computation of $U^L_{I+1/2}$ and $U^R_{I+1/2}$, i.e. the message of this point is *wasted*. Additionally, the base scheme (such as the ordinary third-order upwind scheme) can be optimized by using the dispersion and dissipation optimization techniques [11,12].

In this work, based on the dispersion and dissipation optimization and monotonicity-preserving technique, a second order optimized MUSCL scheme (OMUSCL2) is proposed. Compared with the classical second or third order MUSCL scheme, the new scheme has less dissipation and dispersion and thus has higher resolution for shockwave and small scale waves. The new scheme bears the same stencil and nearly the same computational cost as that of the classical MUSCL scheme, so it is easy to be used or be migrated in the finite volume CFD code.

1 Description of the numerical scheme

1.1 The scalar conservation law

In this section, we start with the description in the one-dimensional case. Consider the scalar hyperbolic conservation law given by

$$\frac{\partial u}{\partial t}+\frac{\partial f(u)}{\partial x}=0. \tag{1}$$

For simplicity, assuming the grids points x_j are uniform, that is, $x_{j+1}-x_j=h$, $x_{j+1/2}=x_j+h/2$. Defined $I_j=[x_{j-1/2},x_{j+1/2}]$ is a uniform partition of the solution domain in space. The semi-discrete conservative scheme of eq. (1) is

$$\frac{\partial u}{\partial t}+\frac{1}{h}(\hat{f}_{j+1/2}-\hat{f}_{j-1/2})=0, \tag{2}$$

where $\hat{f}_{j+1/2}$ is the numerical flux. The details of how to get it will be described in the following. Define

$$L(u)=-\frac{1}{h}(\hat{f}_{j+1/2}-\hat{f}_{j-1/2}), \tag{3}$$

and eq. (2) can be written as:

$$\frac{\partial u}{\partial t}=L(u). \tag{4}$$

In this paper, eq. (4) is discrete in time by the TVD Runge-Kutta scheme [13].

$$\begin{aligned} u^{(1)}&=u^n+\Delta tL(u^n),\\ u^{(2)}&=\frac{3}{4}u^n+\frac{1}{4}u^{(1)}+\frac{1}{4}\Delta tL(u^{(1)}),\\ u^{n+1}&=\frac{1}{3}u^n+\frac{2}{3}u^{(2)}+\frac{2}{3}\Delta tL(u^{(2)}). \end{aligned} \tag{5}$$

1.2 A brief review on MUSCL and TVD property

1.2.1 Van Leer's MUSCL method

In 1979, Van Leer [5] proposed the MUSCL method. Considering eq. (1) and its semi-discrete form eq. (2), many different semi-discrete schemes can be obtained after splitting flux, such as the second-order central scheme, and the second-order or third-order upwind scheme. Different schemes which depend on the expression of $\hat{u}_{j+1/2,L}$ and $\hat{u}_{j+1/2,R}$ can be written in a unified form:

$$\hat{f}_{j+1/2}=f^+(\hat{u}_{j+1/2,L})+f^-(\hat{u}_{j+1/2,R}). \tag{6}$$

A more general form is

$$\begin{aligned} \hat{u}_{j+1/2,L}&=u_j+\frac{1}{4}[(1-k)\delta_x^-+(1+k)\delta_x^+]u_j,\\ \hat{u}_{j+1/2,R}&=u_{j+1}-\frac{1}{4}[(1-k)\delta_x^++(1+k)\delta_x^-]u_{j+1}. \end{aligned} \tag{7}$$

k=−1 is the upwind scheme; k=1 is the central scheme and k=0 is the Fromm scheme. They are all second-order accurate, while k=1/3 is a third-order accurate scheme. If these schemes are used simply, they will produce numerical oscillations. Van Leer [5] improved eq. (7) to

$$\begin{aligned}\hat{u}_{j+1/2,L} &= u_j + \frac{1}{4}[(1-k)\bar{\delta}_x^- + (1+k)\bar{\delta}_x^+]u_j,\\ \hat{u}_{j+1/2,R} &= u_{j+1} - \frac{1}{4}[(1-k)\bar{\delta}_x^+ + (1+k)\bar{\delta}_x^-]u_{j+1}.\end{aligned} \tag{8}$$

where

$$\begin{aligned}&\bar{\delta}_x^+ u_j = \min\mathrm{mod}(\delta_x^+ u_j, b\delta_x^- u_j),\\ &\bar{\delta}_x^- u_j = \min\mathrm{mod}(\delta_x^- u_j, b\delta_x^+ u_j).\\ &1 \leqslant b \leqslant 3,\ \ k = -1,\ \ 1,\ \ 0,\ \ \frac{1}{3}\end{aligned}$$

by reducing significant changes in $\hat{u}_{j+1/2,L}$ and $\hat{u}_{j+1/2,L}$ to improve the ability of capturing shock.

1.2.2 TVD scheme

In 1959, Godunov [14] proposed the monotonicity scheme. Then Jenning [15] proposed the monotonicity–preserving scheme by extending the concept of monotone to non-linear scheme. The numerical solution avoids oscillation near the shock using the monotonicity or monotonicity-preserving scheme.

TVD, first introduced by Harten, means total variation diminishing. The basic idea is to apply the characteristics which are total variation diminishing of differential equations in constructing a difference scheme. In order to construct the TVD scheme, Harten gave a sufficient condition. That is, if the scheme can be written as:

$$u_j^{n+1} = u_j^n + C_{j+1/2}^n(u_{j+1}^n - u_j^n) - D_{j-1/2}^n(u_j^n - u_{j-1}^n), \tag{9a}$$

and for any j satisfies:

$$C_{j+1/2}^n \geqslant 0,\ D_{j+1/2}^n \geqslant 0,\ C_{j+1/2}^n + D_{j+1/2}^n \leqslant 1, \tag{9b}$$

the scheme is a TVD scheme.

1.3 Optimized MUSCL scheme (OMUSCL2) by controlling dispersion and dissipation

1.3.1 Fourier analysis of dispersion and dissipation

The scalar hyperbolic equation (1) is discrete on the stencil $[x_{j-2}, x_{j-1}, x_j, x_{j+1}, x_{j+2}]$. Clearly, five points can construct the 4th order scheme at most. Here five points are used to construct a second-order scheme, then getting a spatial discrete expression with two free coefficients:

$$\begin{aligned}h\frac{\partial f}{\partial x} = &\left(-a - 3b + \frac{1}{2}\right)f_{j-2} + (3a + 8b - 2)f_{j-1}\\ &+\left(-3a - 6b + \frac{3}{2}\right)f_j + af_{j+1} + bf_{j+2},\end{aligned} \tag{10}$$

where a and b are free coefficients.

In order to analyze the dispersion and dissipation errors quantitatively, consider the model problem

$$\frac{\partial u}{\partial t} + c\frac{\partial u}{\partial x} = 0,\ c = \mathrm{const} > 0,$$

with the initial condition:

$$u(x,0) = \mathrm{e}^{ikx}.$$

The exact solution is $u(x,t) = \mathrm{e}^{ik(x-ct)}$. If F_j/h approximates $\left(\frac{\partial u}{\partial x}\right)_j$, then the model problem is written as:

$$\frac{\partial u_j}{\partial t} + c\frac{F_j}{h} = 0, c = \mathrm{const} > 0,$$

with the initial condition:

$$u(x_j,0) = \mathrm{e}^{ikx_j}.$$

Suppose the exact solution of differential equation has the form $u(x_j,t) = \hat{u}(t)\mathrm{e}^{\mathrm{i}k(x_j-ct)}$, then $F_j = K_e\cdot\hat{u}(t)\mathrm{e}^{\mathrm{i}k(x_j-ct)}$ is obtained, $k_e = k_r + \mathrm{i}k_i$. The solution is $u(x_j,t) = \mathrm{e}^{-c\frac{k_r}{h}t}\mathrm{e}^{\mathrm{i}(kx_j - c\frac{k_i}{h}t)}$. Note that k_r=0, k_i=kh for the exact solution. So the dispersion and dissipation errors can be reflected by the functions k_r and k_i [16].

For eq. (10) the functions of dispersion and dissipation are expressed as (kh=α):

$$\begin{aligned}K_r = &\left(\frac{1}{2} - a - 2b\right)\cos(2\alpha) + (4a + 8b - 2)\cos(\alpha)\\ &+\left(\frac{3}{2} - 3a - 6b\right),\\ K_i = &\left(a + 4b - \frac{1}{2}\right)\sin(2\alpha) + 2(-a - 4b + 1)\sin(\alpha).\end{aligned} \tag{11}$$

Define:

$$\begin{aligned}\eta &= 1 - 2a - 4b,\\ \xi &= 2a + 8b - 1.\end{aligned}$$

and eq. (11) is rewritten as:

$$\begin{aligned}K_r &= \eta(\cos^2(\alpha) - 1)^2,\\ K_i &= (1 - \xi + \xi\cos(\alpha))\sin(\alpha).\end{aligned} \tag{12}$$

Here η, ξ are the dissipation and dispersion coefficients, respectively, i.e. the dissipation property of the scheme (10) is determined only by the free parameter η, and the dispersion property of scheme (10) is determined only by the free

parameter ξ. Since ξ and η are independent parameters, the dissipation and dispersion can be the optimized property of scheme (10) independently.

Particularly when $\eta=0$, $\xi=-1/3$, scheme (10) is a fourth-order central scheme.

1.3.2 Optimization for dissipation and dispersion coefficients

Eq. (12) requires $\eta\geqslant 0$ since the dissipation must be positive. In the application of specific physical problem, η can be given an appropriate value to avoid over smoothed discontinuities. So η is a controllable parameter. Here η=0.2 is determined by tests. The following is optimized mainly for dispersion coefficient using the best square approximation method.

The exact value of dispersion is $k_i=\alpha$, by the best square approximation:

$$\begin{aligned}F(\xi)&=\int_0^x(\theta-(1-\xi+\xi\cos(\alpha))\sin(\alpha))^2\,\mathrm{d}\theta\\&=\frac{x^3}{3}+\frac{\xi^3}{8}\left(x-\frac{1}{4}\sin 4x\right)+\frac{(1-\xi)^2}{2}\left(x-\frac{1}{2}\sin 2x\right)\\&\quad+\frac{\xi}{2}\left(x\cos 2x-\frac{1}{2}\sin 2x\right)+2(1-\xi)x\cos x\\&\quad-2(1-\xi)\sin x+\frac{2}{3}\xi(1-\xi)\sin^3 x,\qquad x\in[0,2\pi].\end{aligned}$$

In Table 1, for given x value, ξ value is presented when $F(\xi)$ obtains the minimum value. Figure 1 shows the dispersion curve with different ξ values and the exact value. Figure 1 shows that the dispersion curve will approach exact value better in the range of high wave number as ξ decreases. But Figure 2 shows ξ can't be decreased infinitely. So it is chosen in the range of $\max\left|(\alpha-ki(\alpha)\right|\leqslant 0.05$. Finally $\xi=-0.55$ when $\max\left|(\alpha-ki(\alpha)\right|=0.05$.

As is addressed above, the scheme is the 4th order central scheme when $\xi=-1/3$. Seen from Figure 3, the region is increased by 50% through choosing a new ξ value. That is, for the same resolution, our grid's number is 2/3 of the original fourth-order scheme.

1.3.3 Improving shock capturing ability by adding a TVD limiter

In the above work, $\eta=0.2$ and $\xi=-0.55$ have been defined. So far the scheme is linear, which can't calculate shock. The following is to add a limiter. Flux can be split into $f=f^+ + f^-$, satisfying $\mathrm{d}f^+/\mathrm{d}u\geqslant 0$ and $\mathrm{d}f^-/\mathrm{d}u\leqslant 0$. Consider

Table 1 x and ξ values for minimum $F(\xi)$ value

x	ξ
$\pi/2$	–0.49269
$2\pi/3$	–0.35613
$5\pi/6$	–0.07565

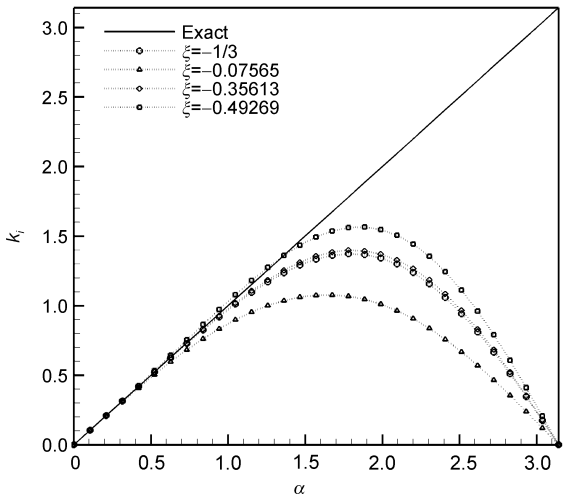

Figure 1 Dispersion curves for different ξ.

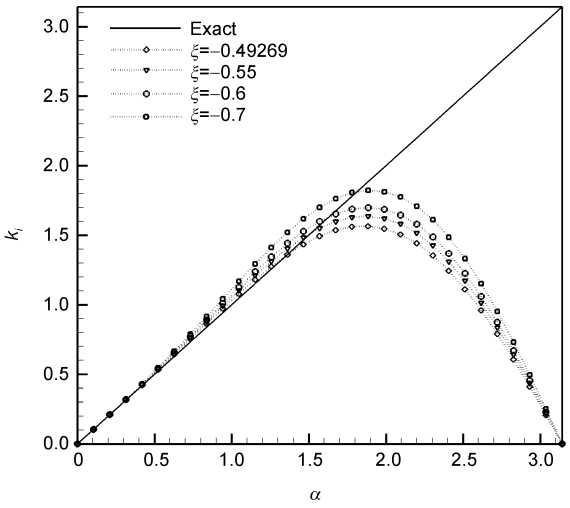

Figure 2 Dispersion curves by decreasing the ξ value.

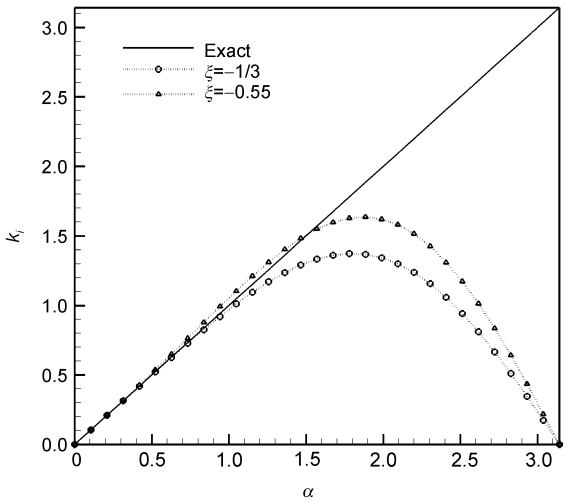

Figure 3 Comparison of $\xi=-1/3$ with $\xi=-0.55$.

eq. (1) only for the case of $\mathrm{d}f^-/\mathrm{d}u = c = \text{ const} > 0$. For the case $c<0$, the scheme is easy to be developed due to the symmetry.

The stencil in the reconstruction of $U_{j+1/2}$ in the classical MUSCL and the new scheme is shown in Figure 4. Classical MUSCL reconstructs left and right states by using three points. Totally four points are used to compute $U_{j+1/2}$, and the message in one additional point is not used, i.e. one point's message is wasted. This inspires us to reconstruct the left and right states by all four points:

$$U^L_{j+1/2} = U^L_{j+1/2}(U_{j-1}, U_j, U_{j+1}, U_{j+2}),$$
$$U^R_{j+1/2} = U^R_{j+1/2}(U_{j-1}, U_j, U_{j+1}, U_{j+2}).$$

So, the new scheme uses the same stencil points in the computation of $U_{j+1/2}$ as that used in the classical MUSCL scheme.

According to the above idea, from eq. (10) we obtain

$$\hat{f}^+_{j+1/2} = \frac{\xi-\eta}{4} f^+_{j-1} + \frac{3\eta-\xi+2}{4} f^+_j + \frac{2-3\eta-\xi}{4} f^+_{j+1} + \frac{\eta+\xi}{4} f^+_{j+2}, \tag{13}$$

where $\xi = -0.55$ and $\eta = 0.2$, which are chosen by the above optimization process.

Based on the limiter technique [17], scheme (13) can be rewritten as a first-order upwind part and a correction part, and then the limiter factor is used in the correction part to keep TVD property. Now, the schemes are

$$\hat{f}^+_{j+1/2} = f^+_j + \frac{1}{\phi_T}\tilde{\phi}_{j+1/2}(f^+_{j+1} - f^+_j),$$
$$\phi_{j+1/2} = 1 - \eta + \frac{\eta+\xi}{2}\frac{1}{r_{j+3/2}} + \frac{\eta-\xi}{2} r_{j+1/2}. \tag{14}$$

Here

$$r_{j+1/2} = \frac{f^+_j - f^+_{j-1}}{f^+_{j+1} - f^+_j}.$$

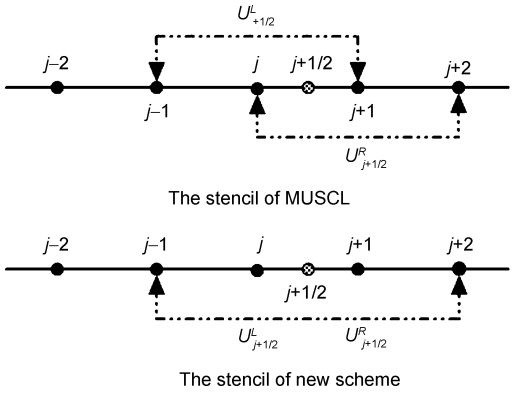

Figure 4 Stencils for the reconstruction of $U_{j+1/2}$.

Ref. [18] demonstrated that this method is identical to the TVD method and gave the range of $\phi_{j+1/2}$:

$$\begin{cases} 0 \leqslant \phi_{j+1/2} \leqslant \dfrac{2}{1-\nu}, \\ 0 \leqslant \phi_{j+1/2} \leqslant \dfrac{2r_{j+1/2}}{\nu}, \end{cases}$$

where ν is the CFL number, and the common value is $0 \leqslant \nu \leqslant 1$.

Finally we choose

$$\tilde{\phi}_{j+1/2} = \max(0, \min(2, \phi_{j+1/2}, 2r_{j+1/2})).$$

Now the OMSCL2 scheme is obtained in the scalar hyperbolic conservation equation. The following will extend it to the Euler equations.

2 Extension to the Euler equations

In this section, the OMUSCL2 method is extended to the Euler equations. The one-dimension Euler equations of gas dynamics can be written as the following conservative form:

$$\frac{\partial U}{\partial t} + \frac{\partial F(U)}{\partial x} = 0,$$

where

$$U = (\rho, \rho u, E)^{\mathrm{T}}$$

is the vector of conservative variables and

$$F(U) = (\rho u, \rho u^2 + p, u(E+p))^{\mathrm{T}}$$

is the vector of flux.

With the idea of MUSCL and TVD, the second-order optimized scheme (OMUSCL2) is got. In order to apply the finite volume method easily and compare it with the MUSCL method, it is rewritten in the same way as the MUSCL method. Here is how to apply this algorithm to the finite volume method.

(1) First, use the OMUSCL2 scheme to compute the left and right states at the face of the control volume $U^L_{j+1/2}$, $U^R_{j+1/2}$:

$$U^L_{j+1/2} = U_j + \frac{1}{2}\tilde{\phi}^L_{j+1/2}\cdot(U_{j+1} - U_j),$$
$$\tilde{\phi}^L_{j+1/2} = \max(0, \min(2, \phi^L_{j+1/2}, 2r^L_{j+1/2})),$$
$$\phi^L_{j+1/2} = 0.8 - 0.175\frac{1}{r^L_{j+3/2}} + 0.375 r^L_{j+1/2},$$
$$r^L_{j+1/2} = \frac{U_j - U_{j-1} + \varepsilon}{U_{j+1} - U_j + \varepsilon},\ r^L_{j+3/2} = \frac{U_{j+1} - U_j + \varepsilon}{U_{j+2} - U_{j+1} + \varepsilon};$$
$$U^R_{j+1/2} = U_{j+1} - \frac{1}{2}\tilde{\phi}^R_{j+1/2}\cdot(U_{j+1} - U_j), \tag{15}$$

$$\tilde{\phi}^R_{j+1/2} = \max(0, \min(2, \phi^R_{j+1/2}, 2r^R_{j+1/2})),$$

$$\phi^R_{j+1/2} = 0.8 - 0.175\frac{1}{r^R_{j-1/2}} + 0.375 r^R_{j+1/2},$$

$$r^R_{j+1/2} = \frac{U_{j+2} - U_{j+1} + \varepsilon}{U_{j+1} - U_j + \varepsilon},\ r^R_{j-1/2} = \frac{U_{j+1} - U_j + \varepsilon}{U_j - U_{j-1} + \varepsilon};$$

where ε is a small value (e.g. $\varepsilon=10^{-6}$).

(2) Then, the fluxes in the face of control volume can be computed by using the flux technique, such as Steger-Warming splitting [19], Van Leer splitting [20], and Roe [21] or the AUSM [22] method.

3 Numerical tests

In this section, this new scheme is used to do some one-dimensional and two-dimensional tests for the sake of comparing it with the original MUSCL schemes.

In the following tests, the original second-order MUSCL scheme (MUSCL2), the third-order MUSCL scheme (MUSCL3) and the new scheme (OMUSCL2) are used to compute the face values, and the Steger-Warming [19] method for one dimension tests and the AUSM-PW [23,24] method for two dimension tests with characteristic-wise are used to compute the flux, The third-order TVD type Runge-Kutta method is used for time advance.

3.1 One-dimensional problems

3.1.1 Several convergence studies for the advection equations [8,25]

The following equation is solved on the domain [−1, 1] with periodic boundary conditions:

$$\begin{cases} u_t + u_x = 0, \\ u(x,0) = \sin(\pi x). \end{cases}$$

The computed L_1 error and order of accuracy are listed in Table 2. The error was measured at t=1 with the CFL number equal to 0.001. Where OMUSCL2 represents the current second-order optimized scheme, MUSCL2 and MUSCL3 represent the second-order and the third-order MUSCL schemes, respectively.

The results in Table 2 tell us that the OMUSCL2 scheme gives the second-order accuracy, which meets the designation order, while the L_1 order of MUSCL2 and MUSCL3 is less than their theoretical order.

3.1.2 Shu-Osher problem [13]

This test indicates that Mach 3 shock interacts with a density disturbance. And this is a good model to test the scheme's resolution for both shocks and fine scale waves. The governing equations are one-dimensional Euler equations and solved on the spatial domain $x \in [0,10]$. The initial conditions are

$$\begin{cases} \rho = 3.857143,\ u = 2.629369,\ p = 10.333333, & \text{when } x < 1, \\ \rho = 1 + 0.2\sin(5x),\ u = 0,\quad p = 1, & \text{when } x \geqslant 1. \end{cases}$$

The solution is advanced up to $t = 1.8$ with 400 points. Since the real exact solution is unknown, the "exact" solution here is obtained by 4000 points. Figure 5 shows the comparison between the OMUSCL2 and MUSCL schemes. Figure 5(b) is the locally enlarged plot of Figure 5(a). The figure shows clearly that OMUSCL2 has better resolution than the original MUSCL schemes, especially, in the region of high wave number.

Table 2 L_1 error and order with $u(x, 0)=\sin(\pi x)$

Method	N	L_1 error	L_1 order
MUSCL2	10	0.3515	-
	20	0.1316	1.42
	40	4.8703×10^{-2}	1.43
	80	1.4067×10^{-2}	1.79
	160	3.8667×10^{-3}	1.86
	320	1.0453×10^{-3}	1.89
MUSCL3	10	0.1867	-
	20	7.8412×10^{-2}	1.25
	40	1.8282×10^{-2}	2.10
	80	4.1645×10^{-3}	2.13
	160	8.7331×10^{-4}	2.25
	320	1.7762×10^{-4}	2.30
OMUSCL2	10	0.1910	-
	20	6.6878×10^{-2}	1.51
	40	2.1127×10^{-2}	1.66
	80	5.5547×10^{-3}	1.93
	160	1.3730×10^{-3}	2.02
	320	3.4528×10^{-4}	2.00

3.1.3 One-dimensional Sod problem [26]

The governing equations are one-dimensional Euler equations, and the computation domain is $x \in [0,1]$. The initial conditions are

$$\begin{cases} \rho = 1, \quad u = 0,\ p = 1, & \text{when } x < 0.5, \\ \rho = 0.125,\ u = 0,\ p = 0.1, & \text{when } x \geqslant 0.5. \end{cases}$$

The solution is advanced up to $t = 0.14$ with 200 points and compared with the exact solution, where the exact solution is computed by using an exact (Godunov) Riemann solver.

The density and velocity distribution obtained by MUSCL schemes and OMUSCL2 are shown in Figures 6 and 7. Where Figures 6(b) and 6(c) are locally enlarged plots of Figure 6(a), Figures 7(b) and 7(c) are locally enlarged plots of Figure 7(a). These figures show that the new scheme produces a better result than the original MUSCL schemes.

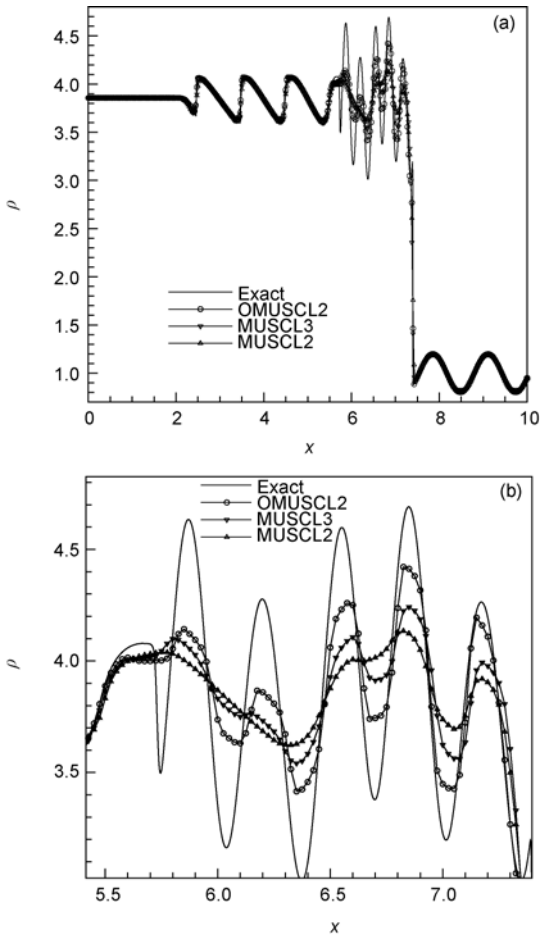

Figure 5 Plots of density at t=1.8. N=400. (b) is the locally enlarged plot of (a).

3.1.4 One-dimensional Lax problem [27,28]

The governing equations are 1D Euler equations and solved on the spatial domain $x \in [0,2]$. The initial conditions are

$$\begin{cases} \rho = 0.445,\ u = 0.698,\ p = 3.528, & \text{when } x < 1, \\ \rho = 0.5,\ \quad u = 0,\ \quad p = 0.571, & \text{when } x \geqslant 1. \end{cases}$$

The solution is advanced up to t=0.32 with 100 points. The density distributions obtained by MUSCL and OMUSCL2 are shown in Figure 8, where Figure 8(b) is the locally enlarged plot. From these figures we can observe that the best solutions are given by OMUSCL2, and the original MUSCL method has more dissipation around the discontinuities and non-physical oscillation.

3.2 Two-dimensional problems

3.2.1 Double Mach reflection problem [29]

The governing equations are two-dimensional Euler equations, and the computational domain for this problem is chosen to be [0, 4]×[0, 1]. Only the region [0, 3]×[0, 1]is used during the computing. The reflecting wall lies at the bottom of the computational domain starting from x=1/6. Initially a right-moving Mach 10 shock in air (γ=1.4) is positioned at x=1/6, y=0, and makes a 60° angle with the x-axis. For the bottom boundary, the region from x=0 to

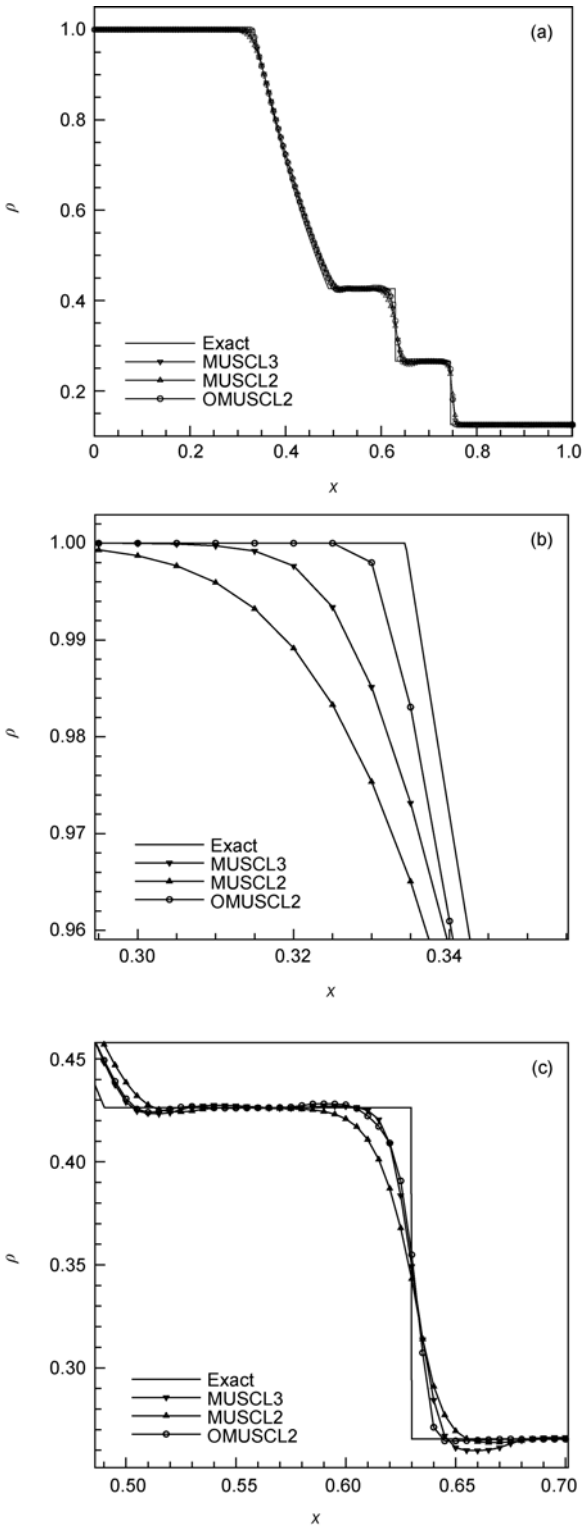

Figure 6 Plots of density at t=0.14, N=200. (b) and (c) are locally enlarged plots of (a).

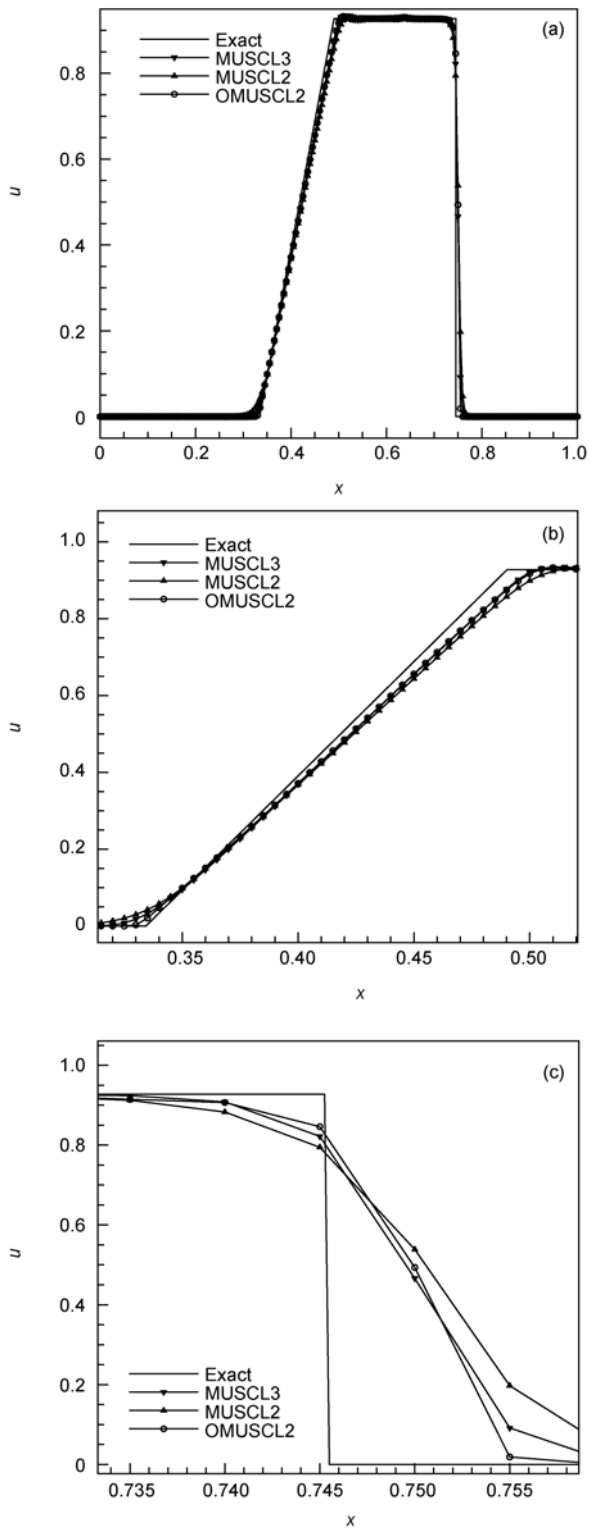

Figure 7 Plots of velocity at t=0.14, N=200. (b) and (c) are locally enlarged plots of (a).

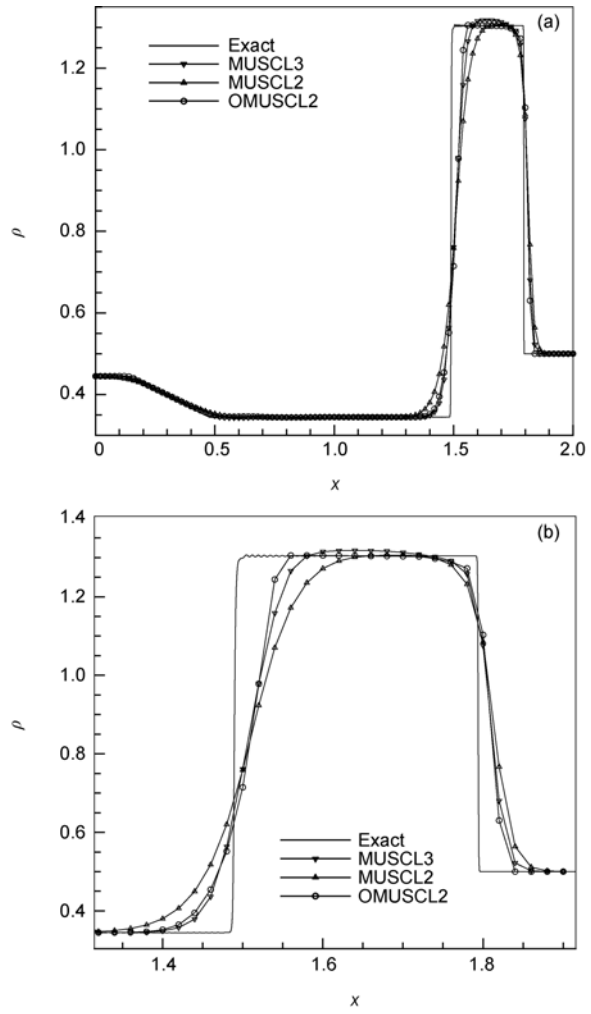

Figure 8 Plots of density at t=0.32, N=100. (b) is locally enlarged plots of (a).

x=1/6 is always assigned the initial values. The boundary with x>1/6 on the x-axis is taken to be a reflecting boundary. At the top boundary of our computational domain, the flow values are set to describe the exact motion of the Mach 10 shock. The problem is run with a CFL number of 0.6 and the results are shown at a simulation time of 0.2. The grid resolution is 960×240 points.

The density distribution obtained by OMUSCL2 is shown in Figure 9, where Figure 9(b) is the locally enlarged plot. The result obtained by MUSCL3 is shown in Figure 10. Figure 9(a) shows that both Mach stems and shocks in this problem are properly captured. By comparing these figures, it's clear that the new scheme (OMUSCL2) achieves a high-resolution in the numerical solution, especially in the region near the Mach stems. The new scheme can capture the rollup of the slip lines which emanate from the head of head clearly. This result also shows that the dissipation of the new scheme is much smaller than that of MUSCL3.

3.2.2 RAE2822 transonic airfoil [30]

The transonic flow over a RAE2822 airfoil is a classical validation test of CFD codes. This airfoil is transonic supercritical airfoil and there's a shock in the leeward side. Numerical solution of the shock position is sensitive to the

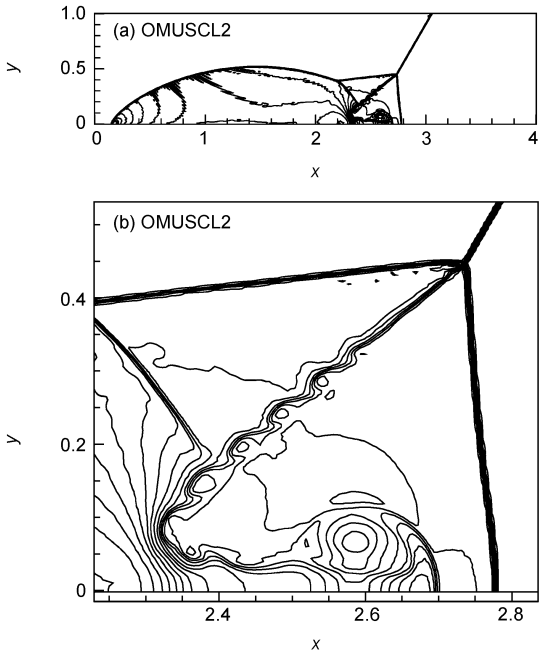

Figure 9 Contours of the density (from 1.731 to 20.92 with 30 equally spaced contours), using OMUSCL2. (b) is locally enlarged plots of (a).

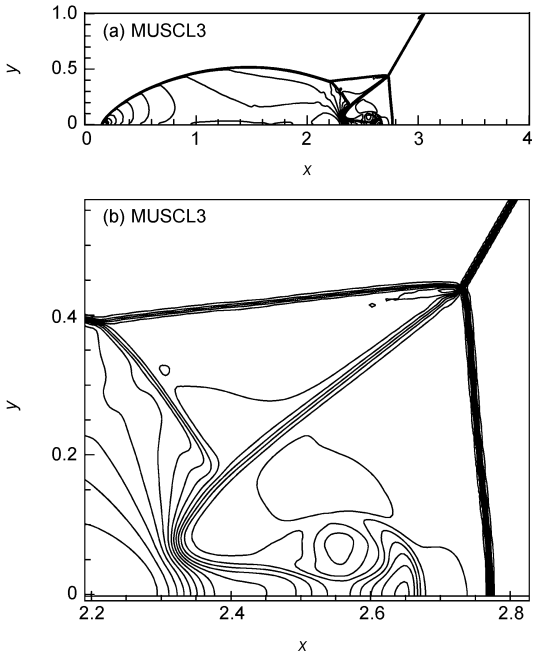

Figure 10 Contours of the density (from 1.731 to 20.92 with 30 equally spaced contours), using MUSCL3. (b) is locally enlarged plots of (a).

numerical methods. So it's a good example to verify the shock resolution of numerical methods.

The grid, a multi-block C-grid, is provided by J.W. Slater from NASA Web[1)]. The total mesh number is 369×69. The grid around the airfoil is shown in Figure 11. The free stream flow conditions are $Ma_\infty = 0.729$; the chord-based Reynolds number is Re=6.5×10^6; the angle of attack is 2.31°. The surface pressure coefficient for the comparison results from [30] (or downloads from the website[1)]).

Figure 12 shows the distribution of the pressure coefficient on the surface of the airfoil. This figure shows that the result of OMUSCL2 is most close to the experimental data, and is better than MUSCL3 and MUSCL2. Especially, the shock's location computed by OMUSCL2 agrees very well with the experimental data. That shows that OMUSCL2 has a higher shock resolution and lower dissipation than the original second-order or third-order MUSCL schemes.

Table 3 gives the CPU time per 1000 steps in this test. The CPU is Intel i7-920 at 2.66 GHz. This table shows that OMUSCL2's computational cost is nearly the same as that of the MUSCL schemes. The new scheme's CPU cost is

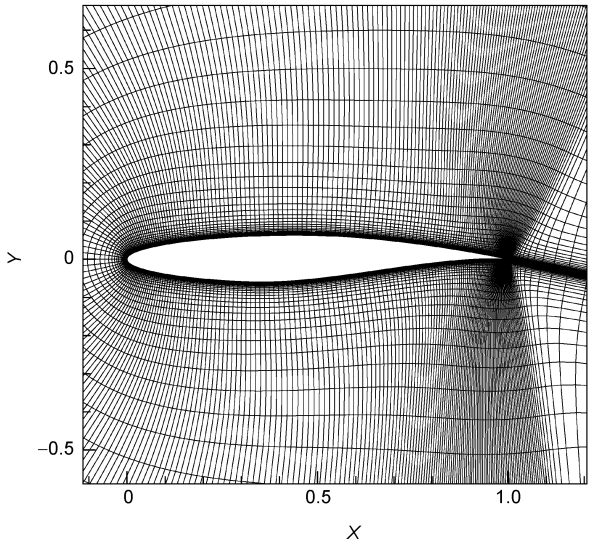

Figure 11 RAE2822 computational grids.

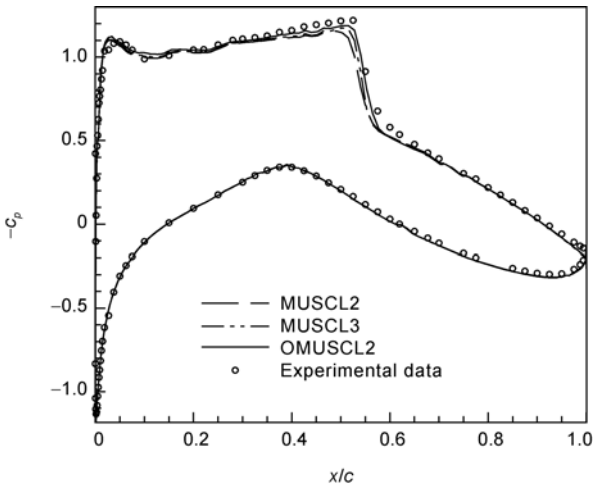

Figure 12 Distribution of the pressure coefficient on the surface of airfoil.

1) http://www.grc.nasa.gov/WWW/wind/valid/raetaf/raetaf.html

Table 3 Comparisons of the CPU time

Scheme	Computational efficiency (per 1000 steps)
MUSCL2	207 s
MUSCL3	215 s
OMUSCL2	224 s

only 8% more than MUSCL2 and only 4% more than MUSCL3. Therefore, the CPU cost can be ignored when the original MUSCL scheme is switched to OMUSCL2 in CFD codes.

4 Conclusion

A second-order optimized monotonicity-preserving MUSCL scheme (OMUSCL2) is developed based on the dispersion and dissipation optimization and monotonicity-preserving technique. The new scheme (OMUSCL2) is simple in expression and is easy to be used in CFD codes. Compared with the original second-order or third-order MUSCL scheme, the new scheme shows nearly the same CPU cost and higher resolution to shockwaves and small- scale waves.

The new scheme is tested through a set of one-dimensional and two-dimensional tests, including the Shu-Osher problem, the Sod problem, the Lax problem, two dimension double Mach reflection and RAE2822 transonic airfoil test. All numerical tests show that, compared with the original MUSCL schemes, the new scheme has lower dispersion and dissipation errors and higher resolution.

Thanks to Professor Ren Yuxin in Tsinghua University for the helpful discussion of the optimization method. Thanks to the National Super computer Center in Tianjin (NSCC) the Supercomputing Center of Chinese Academy of Sciences (SCCAS) and Shanghai Supercomputing Center (SSC) for proving the computing time. This work was supported by the National Natural Science Foundation of China (Grant Nos. 10632050, 10872205, 11072248), the National Basic Research Program of China (Grant No. 2009CB724100), the National High Technology Research and Development Program of China (Grant No. 2009AA010A139), and the Chinese Academy Sciences Program (Grant No. KJCX 2-EW-J01).

1 Harten A. High resolution schemes for hyperbolic conservation laws. J Comput Phys, 1983,49: 357–393
2 Fu D X. Direct numerical simulation of compressible turbulence. Beijing: Science Press, 2010
3 Cada M, Torrilhon M. Compact third-order limiter functions for finite volume methods. J Comput Phys, 2009, 228: 4118–4145
4 Sweby P K. High resolution schemes using flux limiters for hyperbolic conservation laws. SIAM J Numer Anal, 1984, 21: 995–1011
5 Van Leer B. Towards the ultimate conservation difference scheme V. A second-order sequel to Godunov's Method. J Comput Phys, 1979, 32: 101–136
6 Harten A, Engquist B, Osher S, et al. Uniformly high order accurate essentially non-oscillatory shock-capturing schemes III. J Comput Phys, 1987, 71: 231–303
7 Serna S, Marquina A. Power ENO methods: A fifth-order accurate weighted power ENO method. J Comput Phys, 2004, 194: 632–658
8 Jiang G S, Shu C W. Efficient implementation of weighted ENO schemes. J Comput Phys, 1996, 126: 202–228
9 Shu C W. TVB uniformly high-order schemes for conservation laws. Math Comput, 1987, 49: 105–121
10 Suresh A, Huynh H T. Accurate monotonicity-preserving schemes with Runge-Kutta time stepping. J Comput Phys, 1997, 136: 83–99
11 Christopher K W T, Webb J C. Dispersion-relation-preserving finite difference schemes for computational acoustics. J Comput Phys, 1993,107(2): 262–281
12 Lele S K. Compact finite difference schemes with spectral-like resolution. J Comput Phys, 1992, 103: 16–42
13 Shu C W, Osher S. Efficient implementation of essentially non-oscillatory schemes. J Comput Phys, 1989, 83: 32–78
14 Godunov C K. Difference method for computing the discontinuity in fluid dynamics. SB Math+, 1959, 47(3): 271
15 Jennings G. Discrects shock. Comm Pore Appl Math. 1974, 27: 25–37
16 Fu D X, Ma Y W. Computational Fluid Dynamics (in Chinese). Beijing: High Education Press, 2002
17 He Z W, Li X L, Fu D X, et al. A 5th order monotonicity-preserving upwind compact difference scheme. Sci China-Phys Mech Astron, 2011, 54: 511–522
18 Daru V, Tenaud C. High order one-step monotonicity-preserving schemes for unsteady compressible flow calculations. J Comput Phys, 2004, 193: 563–594
19 Steger J L, Warming R F. Flux vector splitting of the inviscid gasdynamic equations with applications to finite difference methods. J Comput Phys, 1981, 40: 263–293
20 Van Leer B. Flux-vector Splitting for the Euler Equations. Technical Report ICASE 82-30, NASA Langley Research Center, USA, 1982
21 Roe P L. Approximate Riemann solvers, parameter vectors and difference schemes. J Comput Phys, 1981, 43: 357–372
22 Liou M S, Steffen J C J. A new flux splitting scheme. J Comput Phys, 1993, 107: 23–39
23 Kim K H, Lee J H, Rho O H. An improvement of AUSM schemes by introducing the pressure-based weight function. Comput Fluids, 1998, 27(3): 311–346
24 Kim K H, Lee J H, Rho O H. An improvement of AUSM schemes by introducing the pressure-based weight function. In: The Fifth Annual Conference of the Computational Fluid Dynamics Society of Canada (CFD 97), 1997. 5: 14-33–14-38
25 Shu C W, Dinshaw S B. Monotonicity preserving weighted essentially non-oscillatory schemes with increasingly high order of accuracy. J Comput Phys, 2000, 160: 405–452
26 Sod G A. A survey of several finite difference methods for system of non-linear hyperbolic conservation law. J Comput Phys, 1978, 21(1): 1–31
27 Shu C W. Essentially Non-Oscillatory and Weighted Essentially Non-Oscillatory Schemes for Hyperbolic Conservation Laws. NASA/CR-97-206253, ICASE Report, 1997: 65–97
28 Toro E F. Riemann Solvers and Numerical Methods for Fluid Dynamics. 2nd. Berlin: Springer, 1997
29 Woodward P, Colella P. The numerical simulation of two-dimens ional fluid flow with strong shocks. J Comput Phys, 1984, 54: 115–173
30 Cook P H, McDonal M A, Firmin M C P. Aerofoil RAE2822- Pressure Distributions, and Boundary Layer and Wake measurements. Experimental Data base for Computer Program Assessment, AGARD Report AR 138, 1979